Evaluating the Effect of Vane Trailing Edge Flow on Turbine Rim Sealing

Iván Monge-Concepción*
Department of Mechanical Engineering
The Pennsylvania State University
University Park, PA 16802, USA
Email: izm4@psu.edu

Reid A. Berdanier
ASME Member
Department of Mechanical Engineering
The Pennsylvania State University
University Park, PA 16802, USA
Email: rberdanier@psu.edu

Michael D. Barringer
ASME Member
Department of Mechanical Engineering
The Pennsylvania State University
University Park, PA 16802, USA
Email: mdb22@psu.edu

Karen A. Thole
ASME Member
Department of Mechanical Engineering
The Pennsylvania State University
University Park, PA 16802, USA
Email: kthole@engr.psu.edu

Christopher Robak
Pratt & Whitney
East Hartford, CT 06118, USA
Christopher.Robak@pw.utc.com

* Corresponding author.

ABSTRACT

Modern gas turbine development continues to move toward increased overall efficiency, driven in part by higher firing temperatures that point to a need for more cooling air to prevent catastrophic component failure. However, using additional cooling flow bled from the upstream compressor causes a corresponding detriment to overall efficiency. A primary candidate for cooling flow optimization is purge flow, which contributes to sealing the stator-rotor cavity and prevents ingestion of hot main gas path flow into the wheelspace. Previous research has identified that the external main gas path flow physics play a significant role in driving rim seal ingestion. However, the potential impact of other cooling flow features on ingestion behavior, such as vane trailing edge (VTE) flow, is absent in the open literature. This paper presents experimental measurements of rim cavity cooling effectiveness collected from a one-stage turbine operating at engine-representative Reynolds and Mach numbers. Carbon dioxide (CO_2) was used as a tracer gas in both the purge flow and vane trailing edge flow to investigate flow migration into and out of the wheelspace. Results show that the vane trailing edge flow does in fact migrate into the rim seal and that there is a superposition relationship between individual cooling flow contributions. CFD simulations using Unsteady Reynolds-Averaged Navier-Stokes (URANS) were used to confirm VTE flow ingestion into the rim seal cavity. Radial and circumferential traverse surveys were performed to quantify cooling flow radial migration through the main gas path with and without vane trailing edge flow. The surveys confirmed that vane trailing edge flow is entrained into the wheelspace as purge flow is reduced. Local CO_2 measurements also confirmed the presence of VTE flow deep in the wheelspace cavity.

INTRODUCTION

Modern gas turbine operation requires that a fraction of the compressor air is bled to provide dedicated flow to cool critical turbine components. These components are subjected to high temperatures and thermal stresses that result in reduced life if not appropriately cooled. The wheelspace cavity is the region located inboard of the main gas path between the rotating disk and the adjacent stationary hardware. This region is subjected to high temperatures due to the continual ingestion of hot gases from the main gas path. To protect the wheelspace, overlapping clearances called rim seals are used to create complex geometries to prevent hot gas ingestion. Although these overlapping clearances can provide some protection from the hot main gas path, it is typically not enough to fully protect the wheelspace. To further protect this region, flow is bled from the compressor and discharged into the wheelspace cavity to keep the cavity purged from hot gas ingestion.

This purge flow is critical to prevent excessive temperatures in the engine's wheelspace which could cause catastrophic engine failure. This flow is increasingly important to gas turbine designers as combustor exit temperatures continue to increase. The purge flow required to fully protect the wheelspace must be enough to prevent hot gas ingestion while at the same time minimize the compressor bled air and the corresponding reduction in gas turbine efficiency.

Researchers have developed ingestion empirical models as well as experimental rigs to validate such models and study turbine rim sealing flow physics. Although there is a general understanding of the physics within simple rim seal geometries, the fluid mechanics associated with more complex geometries and flow conditions in operating gas turbines are not fully understood. For example, the effect of vane trailing edge flow on ingestion and cooling performance has not been

studied in the open literature. Vane trailing edge (VTE) flow is used to cool down the trailing edge of the vane airfoils and also improves aerodynamic performance.

This paper presents a unique study conducted using a turbine test facility with actual engine hardware to investigate the effect of VTE flow on rim cavity cooling effectiveness. It was hypothesized that a change in the main gas path external boundary conditions by adding vane trailing edge flow leads to a change in rim cavity cooling performance. Various purge and VTE cooling flow conditions as well as CO_2 seeding configurations were used to study the individual contributions of each cooling flow in the wheelspace cavity. In addition, surveys in the main gas path were conducted downstream of the one stage turbine to track the radial migration of the purge and VTE flows. By combining rim cavity cooling effectiveness results from the wheelspace as well as CO_2 cooling concentration surveys in the main gas path, the additional cooling benefits of the vane trailing edge flow were quantified. A computational study, using URANS modeling, was also performed to determine both the presence of VTE flow and to identify major fluid structures in the rim cavity region.

LITERATURE REVIEW

Protecting the wheelspace and the rotating disk is key in preventing catastrophic engine failure. Complex rim seal geometries have been developed to prevent hot gas ingestion into the vulnerable wheelspace cavity. Although extensive research has been performed over decades, only a few empirical models are available to engine designers to predict the purge flow required to minimize hot gas ingestion into the wheelspace.

Reviews performed by Scobie et al. [1] and Johnson et al. [2] outline previous research on ingestion mechanisms in the rim seal. The most important flow mechanisms described include

rotationally-induced effects driven by disk pumping, and externally-induced effects due to pressure asymmetries in the main gas path annulus. The pressure asymmetries are caused by the vane exit potential field that varies from the vane suction-side to the vane pressure-side, and by the rotating blade pressure field that varies from the blade stagnation location to the flow passage. Regions in the main gas path annulus at the vane exit that exhibit relatively high pressure drive the ingress flow towards regions of relatively low pressure in the wheelspace. Similarly, for regions in the main gas path annulus that exhibit relatively low pressure, egress flow occurs from the wheelspace. As previously discussed, no definitive literature exists that discusses the specific effect that the VTE flow has on rim seal ingestion behavior; however, relevant literature on rim seal ingestion mechanisms will be summarized in this section.

Initial experiments carried out by Bayley and Owen [3] used simplified geometries for shrouded and unshrouded disks. The authors were able to study egress and ingress mechanisms as well as draw correlations on the minimum flow rate required to fully purge the wheelspace cavity. Phadke and Owen [4–6] wrote a three-part paper on rim sealing aerodynamics that describes the physics of rotationally-induced and externally-induced ingestion using simplified geometries without airfoils. The authors found that double-shrouded radial clearance seals provide more advantages in preventing ingestion compared to other rim sealing geometries.

Empirical models have been developed based on studies using simplified disk geometries. One of the most widely used models was developed and described by Owen [7] as an orifice model. The orifice model consists of treating rim sealing as two orifices in which part of the flow ingresses and another part of the flow egresses the rim seal region. Their paper describes and derives the orifice equations in which the viscous effects are negligible when compared to the inertial effects. The orifice model quantifies rim sealing effectiveness as a non-dimensional discharge coefficient.

Owen et al. [8] later used computational fluid dynamics (CFD) analyses to test and confirm that externally induced ingestion is mainly due to the magnitude of the peak-to-trough circumferential difference of pressure in the turbine annulus. Their results agreed with Owen's previous studies on externally induced ingestion. It should be noted that most public literature lists externally-induced ingestion as the most important mode of ingestion and as such has received much attention.

Sangan et al. [9] carried out experiments using vanes and symmetric NACA 0018 blade airfoils to study externally-induced modes of ingestion in engine-representative geometries. The experimental data suggests that using the simple orifice model by Owen, it was possible to predict the minimum purge flow required to fully seal the wheelspace cavity. The data also illustrates it can be correlated using a non-dimensional sealing parameter, Φ_0.

Using the continuous-duration turbine test facility described by Barringer et al. [10] several studies were conducted on rim sealing using engine-realistic geometries at engine-relevant conditions in both rotational and axial Reynolds numbers, as well as Mach numbers. Experiments performed by Clark et al. [11] evaluated two vane purge flow configurations including 150 and 32 purge delivery holes, over a range of purge mass flow rates. The authors found that previous empirical models developed by Owen can both under- and over-predict rim sealing effectiveness for realistic rim seal geometries. Clark et al. [12] found that Owen's orifice model was able to predict rim sealing effectiveness in the outer rim seal, but it was unable to accurately predict sealing effectiveness in the region of the purge flow injection holes. Berdanier et al. [13] compared sealing effectiveness for part-span turbine airfoils and full-span turbine airfoils at engine-relevant conditions. Results showed that previous experiments were scalable between different span heights if the minimum required purge flow rate to fully seal the wheelspace cavity, $\Phi_{\min}$, is known. The

authors also found an inflection in the rim sealing effectiveness behavior at the rim seal location in both engine spans. This inflection has also been reported by other authors in previous studies [14–17].

Scobie et al. [18] studied ingress and egress in a 1.5-stage turbine test rig and quantified the egress flow from the upstream wheelspace cavity that is ingested into the downstream wheelspace cavity. In their study, the authors used effectiveness measurements and radial traverses upstream and downstream of the turbine blade to study the effects of cooling flow being "carried-over" into the following wheelspace cavity by re-ingestion. The authors found that the upstream purge does not disturb the fluid dynamics significantly and instead partially mixes with the annulus flow near the downstream seal. Finally, the authors observed that flow carried over from an upstream rim seal to a downstream seal could significantly reduce the adverse effect of ingress in the downstream wheelspace.

Horwood et al. [19] used CO_2 as a tracer gas to study cooling flow migration in the annulus with radial traverses between the stator and rotating blades as well as aft of the rotating blades. The authors used CFD as well as rig experiments to study cooling flow migration and structures. They observed that cooling flow coming from a completely purged cavity is entrained into the passage vortex on the suction side of the blade.

The goal of the research presented in this paper is to assess main gas path ingestion behavior and rim cavity cooling performance in the presence of both purge and vane trailing edge cooling flows using engine-representative geometries at engine-relevant conditions. Although there have been many studies on the performance of purge flows in the wheelspace cavity and the aerodynamic effects of vane trailing edge flow [20, 21], a public study on ingestion and rim cavity cooling performance in which both cooling flows are present together has not been completed.

EXPERIMENTAL METHODS

Experiments presented in this paper were performed in the test turbine located at The Pennsylvania State University's Steady Thermal Aero Research Turbine (START) Lab. The START Lab includes a continuous, steady-state turbine rig that operates with engine-representative hardware at engine-relevant Reynolds and Mach numbers. The facility was designed to study and improve upon engine cooling technologies that will be used in future gas turbines, improve relevant instrumentation, and implement additive manufacturing solutions.

Figure 1 illustrates a summary of the facility's major equipment as well as recent upgrades. Two industrial compressors powered by dedicated 1.1 MW (1500 hp) motors supply the facility with compressed air for both the main gas path (MGP) and the secondary cooling air paths. Each of the compressors has an air flow discharge capacity of 480 kPa and 395 K (70 psi and 250°F) that results in a total turbine airflow capability of 11.4 kg/s (25 lbm/s). The secondary cooling air is thermally conditioned by a chiller to temperatures as low as 273 K (32°F) and subsequently flows to multiple independently controlled and metered air flow lines. The compressed air flowing into the main gas path is heated to the testing condition using a 3.5 MW in-line natural gas heater. This capability provides enough heating to raise the air temperature from 395 K up to 672 K (250°F to 750°F). Details of the facility design and recent expansion have been described by Barringer et al. [10] and Berdanier et al. [13].

Figure 2 shows a summary of the secondary cooling air paths, main gas path, and wheelspace locations. The secondary cooling air system consists of three independently controlled air flow paths. The system delivers cooling supply air to the (a) purge flow plenum located in the inner cavity of the first vane, (f) vane trailing edge flow plenum located in the outer annulus above the first vane, and (h) tangential on-board injection (TOBI) flow. The purge flow provides the

wheelspace and rim cavity regions with a constant supply of cooling flow through 150 equally spaced holes in the circumferential direction. It should be noted that although TOBI flow capability was built into the design of the test facility, TOBI flow was not used in this study. The inner and outer vane plenum cavities were sealed and isolated from one another. Vane trailing edge flow spans radially from the vane hub to vane tip.

Facility Instrumentation and Circumferential Traverse

For the current study, four additively manufactured vanes, produced using direct metal laser sintering (DMLS) nickel alloy, were included in the vane ring assembly since the manufacturing method provided the ability to spatially position pressure taps at precise locations in the main gas path, rim seal region, and rim cavity region. The manufacturing method also allowed integrated internal routing tubes to connect the pressure taps to pressure transducers and CO_2 gas analyzers using Teflon tubing. The four vanes were spaced in the vane ring assembly with two vanes in each opposing side of the vane ring. Engine-run vanes were used alongside the additively manufactured vanes. The film cooling holes in the engine-run vanes were sealed closed using epoxy and only the vane trailing edge holes were left open to provide the correct aerodynamic boundary condition between the vanes and blades.

Figure 3 shows the turbine instrumentation and measurement locations used throughout this study. Single element Kiel pressure probes measured inlet pressure and background main gas path CO_2 concentration entering the turbine, which was important because the inline heater combustion process contributed to the background CO_2 level. Static pressure taps were also used in the inner and outer diameter plenums of the first stage vane to measure the purge flow and VTE flow pressures and CO_2 concentrations. Temperature probes were also located in both plenums. A series

of pressure taps were included in the additively manufactured (AM) vanes. The taps were located in both the radial and circumferential directions which allows for pressure and CO_2 sampling in the rim seal, rim cavity, and wheelspace cavity.

For the current study, a traverse system capable of moving both circumferentially and radially was installed at the turbine outlet to map radial migration of the coolant flows in the main gas path. The circumferential traverse had the capability of moving a total of 2.3 vane pitches and was installed 5.6 axial blade chords downstream of the blade's trailing edge. The radial traverse system was designed to move probes through the full radial span of the main gas path annulus. For this particular study, the radial traverse was configured to limit movement from 5% to 100% radial span. This span limitation was used to accommodate the head of the Kiel probe to prevent accidental contact at the inner turbine wall. To measure the coolant flow migration, CO_2 concentration levels were measured using a 1.6 mm (0.063 in) diameter Kiel probe.

CO_2 Tracer Gas Concentration

To study main gas path ingestion into the rim seal and cooling flow radial migration, CO_2 tracer gas was injected into the secondary cooling flow supply paths. Conventional rim sealing effectiveness, ε, is a mass transfer based analysis that evaluates how effective a seal design is in preventing main gas path flow ingestion into the rim seal for varying amounts of cavity cooling purge flow. The CO_2 gas is typically injected at a small mass fraction (1%) of the total cooling flow and is used as a gas tracer to determine where and how much cooling flow makes its way to a certain location in the wheelspace.

The CO_2 gas is used as a proxy for mass transfer, and gas concentration measurements are therefore used to determine sealing concentration effectiveness (ε_c). The conventional definition

of rim sealing effectiveness and sealing concentration effectiveness takes into account the wheelspace cooling flow source concentration level, c_s, and the main gas path concentration level, c_∞, at the rim seal entrance. When the vane trailing edge cooling flow is introduced and is also seeded with CO_2 at a level different than c_∞, the local main gas path concentration level at the rim seal entrance is affected. The VTE flow locally partially mixes with the background main gas path flow. By the time this mixed flow reaches the rim seal entrance, if the VTE flow is seeded with CO_2 at a level different than c_∞, the conventional definition of rim sealing has been affected. Therefore, to continue using the conventional definition of rim sealing concentration effectiveness the locally mixed background concentration value is needed at the rim seal entrance. This locally mixed value however is not known, is not constant in the radial and circumferential directions, and the amount of the VTE flow that is ingested is unknown.

For this purpose, a new parameter is presented called rim cavity cooling effectiveness (ε_{cc}). The rim cavity cooling effectiveness is given by Equation (1). This cooling effectiveness level will vary between the range of zero and one, in which a value of zero corresponds to the main gas path flow condition at the turbine inlet and a value of one corresponds to the cooling flow source condition.

$$\varepsilon_{cc} = \frac{c - c_{\infty,in}}{c_s - c_{\infty,in}} \tag{1}$$

To calculate the rim cavity cooling effectiveness, a CO_2 molar concentration by volume measurement, c, is measured from one of the discrete pressure taps or Kiel pressure probe. Main gas path background at the turbine inlet, $c_{\infty,in}$, and cooling air supply, c_s, concentrations were also obtained from pressure taps in the vane plenums as well as with a Kiel pressure probe at the turbine inlet. Rim cavity cooling effectiveness must not be confused with the conventional definition of

rim sealing effectiveness, ε_c. Rim cavity cooling effectiveness takes into account the cooling source purge flow that originates from within the wheelspace as well as the cooling source VTE flow that originates from the main gas path, whereas conventional rim sealing effectiveness includes only the cooling source flow from the wheelspace. The CO_2 concentration of the air exiting the heater and thus entering the turbine was also required since the combustion process increased the amount of CO_2 levels in the main gas path flow to nearly 5 times higher than the ambient atmospheric CO_2.

The CO_2 gas was injected into the secondary air flow lines as shown in Figure 4. Both the vane purge and vane trailing edge flows were seeded independently with varying CO_2 levels, the level of which depended on the flow configuration that was studied. The CO_2 samples are extracted from the turbine test section following the validation method outlined by Clark et al. [22]. Sampling is performed by extracting flow so that the extraction rate maintains an "iso-kinetic" condition.

Turbine Operating Point

The data presented in this paper constitutes data gathered from a single-stage full-span turbine that includes vane under platform purge flow as well as vane trailing edge flow. This study presents local cooling flow concentration versus scaled cooling flow rates, Φ/Φ_{ref}, where Φ is the cooling flow rate of purge or VTE flow and Φ_{ref} is the reference flow rate defined as the purge flow rate at which the front rim cavity was fully sealed in the Baseline configuration at Location B in Figure 5. By definition, for a fully sealed front rim cavity ($\varepsilon_c = 1$), the scaled purge flow rate $\Phi_{\mathrm{P}}/\Phi_{\mathrm{ref}}$ equals to one. All flow rates, pressures, and temperatures were held constant with relative

variations of less than 0.7% operating continuously within a span of several hours. Other related conditions are defined in Table 1.

Uncertainties for related test parameters are included in Table 2. The reference conditions in Table 1 are the maximum capability of the turbine facility described by Berdanier et al. [13]. The uncertainty analysis was performed according to the method of Figliola and Beasley [23] and the values reported include both the bias and precision uncertainties for each measurement. Gas analyzer bias uncertainty was reduced by calibrating the gas analyzer with a 0% CO_2 concentration bottle and a 1% CO_2 concentration bottle. CO_2 concentration precision was minimized by averaging CO_2 data collected over a 20-second time window. Repeatability of CO_2 concentration measurements was within $\varepsilon_c = \pm 0.015$.

Rim Seal Test Locations and CO_2 Seeding Configurations

Rim seal testing was conducted at the four radial locations in the stator-rotor interface shown in Figure 5. These locations include the front rim seal (Location A), outer front rim cavity (Location B), inner front rim cavity (Location C) and the front wheelspace cavity (Location D).

To systematically evaluate the effect of VTE flow on rim cooling performance, a series of controlled CO_2 seeding configurations was developed. Figure 6 shows a visual representation of the seven configurations. This methodology required independent injection of the CO_2 tracer gas into each of the two cooling flow paths so that the cooling flow CO_2 level could be matched to the main gas path CO_2 level for certain cases. The first of seven configurations shown in Table 3 represents a *Baseline* configuration in which only the main gas path flow and purge flow were present. The *Baseline* configuration included the main gas path flow at the background 0.2% CO_2 level and the rim cavity purge flow at an elevated 1.0% CO_2 level and no VTE flow. The *Baseline*

configuration was used to study rim sealing effectiveness for purge mass flow rates varying from $\Phi_P/\Phi_{ref} = 0.1$ to 1.33.

The second CO_2 seeding configuration referred to as the *Purge* configuration is similar to the *Baseline* configuration with the difference being that VTE flow is turned on at a constant mass flow ratio of $\Phi_{VTE}/\Phi_{ref} = 0.4$ and the CO_2 concentration is matched to the main gas path flow ($c_{\infty,in}$). The objective for the *Purge* configuration was to establish the effect that the VTE flow has on the rim seal since the VTE flow sets up an engine relevant boundary condition. Because the *Purge* configuration has the VTE flow with a CO_2 concentration matched to that of the main gas path, thereby making the VTE flow indistinguishable from the main gas flow, any changes to the rim cavity cooling effectiveness levels are a result of the change in the external boundary condition and/or a result from any VTE flow entering the rim seal area since the CO_2 level is low.

The third CO_2 seeding configuration referred to as the *Purge+VTE* also includes VTE flow at a mass flow ratio of $\Phi_{VTE}/\Phi_{ref} = 0.4$ but with the difference being that the VTE CO_2 concentration level is matched to that of the purge flow (c_s). The objective of this particular configuration was to evaluate the combined cooling effect of purge and VTE flow in the wheelspace cavity.

The fourth and fifth CO_2 seeding configurations, referred to as *VTE1* and *VTE2*, included background CO_2 levels for the purge flow with an elevated CO_2 level for the VTE flow. The objective for the *VTE1* and *VTE2* configurations was to quantify the sole influence of VTE flow in the wheelspace cavity. By having the purge flow "invisible", since it is matched to the main gas path CO_2 level ($c_{\infty,in}$), any significant CO_2 levels in the rim seal result from the VTE flow. The difference between the *VTE1* and *VTE2* configurations was the mass flow ratios used. The *VTE1* configuration operated at the same purge and VTE mass flow rates as the *Purge* and *Purge+VTE*

configurations. The *VTE2* configuration held the purge mass flow rate constant at $\Phi_P/\Phi_{ref} = 0.4$ while the VTE mass flow rate was varied from $\Phi_{VTE}/\Phi_{ref} = 0.1$ to 0.7.

The sixth CO_2 seeding configuration referred to as *VTEMigration* includes VTE and purge flow rates seeded at the elevated 1% CO_2 level. The *VTEMigration* studies purge flow at a constant mass flow ratio of $\Phi_P/\Phi_{ref} = 1.2$, which corresponds to a fully purged cavity ($\varepsilon_c = 1$), while the VTE mass flow varies from $\Phi_{VTE}/\Phi_{ref} = 0.0$ to 0.7. The objective of this configuration was to evaluate the VTE flow migration in the main gas path for a fully purged cavity condition.

The seventh CO_2 configuration referred to as *PurgeMigration* also includes VTE and purge flows seeded at the elevated 1% CO_2 level. Contrary to *VTEMigration*, *PurgeMigration* flows VTE at a constant mass flow ratio of $\Phi_{VTE}/\Phi_{ref} = 0.4$ while varying the purge mass flow ratio from $\Phi_P/\Phi_{ref} = 0.3$ to 1.2. The objective of this configuration was to study the flow migration of the purge flow for a nominal VTE mass flow rate.

RIM COOLING EFFECTIVENESS RESULTS

The *Baseline* study was performed to benchmark the turbine at the operating point with only vane purge flow (no VTE flow) and the results are shown in Figure 7. In the *Baseline* study, rim sealing effectiveness data is presented since one cooling flow source, purge flow, is present and the conventional definition of rim sealing effectiveness applies. The current results were found to be consistent with those previously published by Berdanier et al. [13]. For each wheelspace radial location, there are various pressure taps on the stator side. Data shown in Figure 7, and subsequent figures, were plotted by arithmetically averaging the concentration measurements in all pressure taps for a particular radial location at a specified purge and/or VTE flow rate.

Rim sealing effectiveness was found to increase with increasing purge mass flow rate. As expected, rim sealing effectiveness levels are higher at locations deeper in the cavity (Locations B, C and D). It can also be observed that these locations achieve a fully purged condition at lower purge flow rates compared to the front rim seal (Location A). The data indicates a fully purged front rim seal cavity (Location B and C) at $\Phi_P/\Phi_{ref} = 1.0$ purge flow rate as defined previously.

In Figure 8, the rim cavity cooling effectiveness results are shown for the *Purge* seeding configuration with the objective of understanding the influence of the VTE flow boundary condition being present. Results in Figure 8 show that rim cooling effectiveness is reduced for the *Purge* configuration compared to the *Baseline* results particularly for locations deeper into the cavity. It was hypothesized that this lower rim cooling effectiveness behavior may not be due to poor rim cooling performance caused by the presence of the VTE flow boundary condition, but rather that the VTE flow may be entering the rim seal and cavity regions. If the VTE flow is being ingested into the rims seal, the CO_2 concentration (for this seeding configuration) in the cavity would be reduced due to dilution of the 1.0% CO_2 seeded purge flow by the 0.2% CO_2 seeded VTE flow. The subsequent CO_2 seeding configurations were used to validate this hypothesis.

For the *Purge* seeding configuration, the rim seal (Location A) was found to have nearly the same cooling effectiveness with the presence of the VTE flow boundary condition, as shown in Figure 8. However, rim cooling effectiveness at locations deeper in the cavity were affected by the presence of the VTE flow.

The *Purge+VTE* configuration helped to address the question of whether VTE flow was being ingested into the rim seal and down into the cavities. Figure 9 shows that rim cavity cooling effectiveness increases for the *Purge+VTE* case relative to the *Baseline* case. The VTE flow has a positive effect on rim cooling effectiveness, and this effect is thought to be a result of the cool air

exiting the vane trailing edge being ingested into the rim seal and wheelspace. This finding is unique since there are no public studies that demonstrate that VTE flow has a positive effect on rim cooling effectiveness. This result is important because of the direct relevance to the operation of a turbine since it implies that there is assistance from the VTE cooling flow in ensuring the under-platform hardware does not reach catastrophic temperatures.

One difference found between the *Purge* and *Purge+VTE* CO_2 seeding configurations is the effect VTE flow has on the rim seal region Location A. In the *Purge* configuration, the Location A cooling effectiveness did not change whereas the deeper locations in the wheelspace showed decreased levels. However, for the *Purge+VTE* configuration the rim cooling effectiveness increased at Location A when VTE flow was seeded at the same elevated 1.0% CO_2 concentration as the purge flow (c_s). This phenomenon difference has been confirmed to be repeatable at various flow and CO_2 seeding configurations and further studies are needed to fully understand this observation.

To fully prove whether VTE flow is ingested into the rim seal and cavities, two additional seeding configurations were used to study the sole influence of VTE flow on rim cooling effectiveness. Recall that the *VTE1* seeding configuration sets the purge flow at the same low 0.2% background level of CO_2 as the main gas path ($c_{\infty,\mathrm{in}}$) and only seeds the VTE flow at an elevated level ($c_s = 1\%$) thus establishing the VTE flow as the dominant CO_2 source. Any measurements within the rim seal and cavities indicating CO_2 levels above the background level ($c_{\infty,\mathrm{in}}$) are therefore a direct result of the VTE flow entering the rim seal and cavity regions. Figure 10 represents to what direct extent the VTE flow enters and influences the rim cooling performance as the purge flow mass flow ratio is increased. It can be seen that as purge flow is increased, the influence of VTE flow decreases. With increasing purge flow, the purge flow dominates the flow

field in the wheelspace cavity. The *Baseline* study showed that at $\Phi_P/\Phi_{ref} = 1.0$ to 1.3, the wheelspace is fully purged and thus the amount of VTE flow that is ingested is minimal.

Although the *Purge* and *VTE1* CO_2 seeding configurations are different, there is a similarity between them. In the *Purge* configuration, the deeper wheelspace cavity locations appear to be the most influenced by the presence of VTE flow. From observation of Figure 10, it can be seen that the front rim seal (Location A) is again the least influenced by the presence of VTE flow. The highest rim cooling effectiveness that the Location A front rim seal is able to achieve for the *VTE1* configuration is close to 10% ($\varepsilon_{cc} = 0.1$). This approximate 10% effectiveness is at the lowest purge flow used in this study. Deeper wheelspace radial locations are able to achieve 25-30% rim cooling effectiveness levels at the same lowest purge flow rate.

For the *VTE2* seeding configuration, the purge mass flow was held constant while the VTE mass flow ratio was varied. The VTE mass flow rate was varied from $\Phi_{VTE}/\Phi_{ref} = 0.1$ to 0.7 while holding the purge mass flow ratio constant at $\Phi_P/\Phi_{ref} = 0.4$. Figure 11 shows that increased VTE flow results in increased cooling performance and confirms that VTE flow makes its way into the wheelspace. The locations that are deeper in the cavity (Locations B, C and D) show a similar increase in rim cavity cooling effectiveness behavior to one another. The rim seal (Location A) however does not experience as sharp a rise in rim cooling effectiveness as locations deeper in the cavity, which is consistent with the Purge configuration where the deeper cavity locations are more affected by the presence of the VTE flow.

From Figure 11 it can be observed that for Locations B, C and D cooling effectiveness increases at the same rate. Location A cooling effectiveness increases at a lower rate when compared to wheelspace locations deep in the cavity. This behavior is consistent to previous results shown in Figure 8 and Figure 10. The *Purge* and *VTE1* configurations results indicated that VTE

flow influence in the rim seal cavity (Location A) is low when compared to deeper cavity locations (Locations B, C and D). This is consistent with results from *VTE2* configuration where VTE flow influence is low at Location A as VTE flow ratio increases. It is believed that rim cavity cooling effectiveness results in Location A are affected because flow is ingested on the rotor side instead of the stator side as suggested by conventional CFD models. Flow ingestion on the rotor side and egress occurring on the stator side was observed using URANS and LES computational simulations in a study by Gao et al. [24]. Since flow enters the rim seal on the rotor side, the pressure taps in the rim seal on the stator side at Location A are not able to capture fully mixed concentration measurements. As flow continues deeper into the cavity regions, it continues to mix, and an expected cooling effectiveness change is reflected.

COMPUTATIONAL SIMULATION OF VTE FLOW INGESTION

A computational fluid dynamics (CFD) simulation was performed to better understand the VTE ingestion flow physics. The computational domain modeled includes the geometry of the 1st vane and 1st blade airfoils. The rim seal cavity geometry was modeled to match the experiment's geometry and capture the flow migration from the rim seal cavity to the blade under-platform cavity and out of the blade damper seals.

A quarter wheel CAD geometry was meshed using commercial software [25]. The mesh was then exported to a commercial CFD code [26] for further simulation and analysis. To fully capture the VTE flow ingestion physics into the rim seal, a high-fidelity Unsteady Reynolds-Averaged Navier-Stokes (URANS) solver was used. The turbulence model selected for this study was the K-Omega SST model. Further details of the meshing process, turbulence model settings, and equations of state can be found in Robak et al. [27].

For this computational study, the test condition chosen was a purge flow ratio of $\Phi_P/\Phi_{ref} = 0.4$ and VTE flow ratio of $\Phi_{VTE}/\Phi_{ref} = 0.4$. This test condition was chosen because experiments indicated that the cavity is not fully sealed but that both flows affect the rim cavity cooling effectiveness. Figure 10 shows that at $\Phi_P/\Phi_{ref} = 0.4$ the influence of VTE flow on rim cooling effectiveness is high. These boundary conditions are used to visualize the mixing taking place in the rim seal cavity between the VTE flow and the rim seal cavity.

Figure 12(a) shows the trailing edge of the 1st stage vane including the vane platform, front rim seal (FRS), front rim cavity (FRCA and FRCB) and the purge holes. The figure depicts the presence of VTE flow (red) coming from the main gas path and non-VTE flows depicted as blue which includes the main gas path (MGP) and purge flow coming from the purge holes.

As flow exits the VTE, it partially mixes along the trailing edge with the main gas path. The flow nearest to the inner vane hub wall slowly mixes with the main gas path and moves along the hub wall as shown in Figure 12(a) before becoming entrained into the rim seal. Most of the mixing occurs at the hub near the entrance of the rim seal in the vane platform area. Figure 12(b) shows a cross-sectional view of the main gas path and rim cavity region. In this region, flow streamlines and velocity vectors are plotted on top of the presence of VTE flow in the main gas path and the rim cavity region. Figure 12(b) shows that a recirculation zone develops at the interface of the vane platform and the turbine rotor disk. Mixing takes place in this recirculation zone and continues as VTE flow is further ingested inward, toward the front rim seal.

The simulation shows that flow present in the front rim seal (FRS) recirculates and that ingress occurs on the wall of the stator whereas egress occurs along the rotor wall. This result contrasts with the previous statement that suggests ingress along the rotor wall and egress on the stator wall as explained by Gao et al. [24]. Looking carefully at Figure 12(b), there appears to be flow

separation on the midspan of the FRS. This separation is in front of the pressure tap where CO_2 concentration is measured, which may explain why the FRS measurements appear to have the least effect of VTE flow being ingested. Regardless, further work is needed to fully explain why the FRS taps are the least affected by the VTE flow.

As VTE flow is entrained inward into the rim seal cavity, it continues to mix with the purge flow as shown in Figure 12. The CFD simulation shows that VTE flow is present at every measurement tap location and that VTE flow can be found as deep as the front wheelspace cavity (FWSC), which is in agreement with the measurements presented in Figure 11.

SUPERPOSITION OF PURGE AND VTE FLOWS

Given the various seeding configurations shown in Table 3, it was possible to evaluate whether a simple linear superposition relationship exists between the effectiveness with and without the VTE flow. As stated previously, the CO_2 seeding configurations *Purge*, *Purge+VTE* and *VTE1* all share the same secondary air mass flow rates. Equation (2) shows a potential superposition relationship.

$$\varepsilon_{\text{Purge+VTE}} = \varepsilon_{\text{Purge}} + \varepsilon_{\text{VTE1}} \tag{2}$$

By subtracting the rim cavity cooling effectiveness data of the Purge configuration (Figure 8) from the rim cavity cooling effectiveness data of the *Purge+VTE* configuration (Figure 9) the results were evaluated to determine whether they yield the same results as those measured for the *VTE1* configuration (Figure 10).

Figure 13 confirms that there is a linear superposition relationship between the seeding configurations. The solid symbols show the results of subtracting the Purge data from the *Purge+VTE* data, and the open symbols show the measured results for the *VTE1* configuration.

This figure shows that using the results of the *Purge* and *Purge+VTE* configurations the direct influence that the VTE flow has on the rim cavity cooling effectiveness can be accurately predicted. This superposition relationship is also an independent verification that the measured cooling effectiveness levels are repeatable.

FLOW MIGRATION INTO THE MAIN GAS PATH FLOW

Flow that has egressed from the stator-rotor wheelspace cavity has the potential of migrating into the main gas path. This egressed flow was shown to provide a tangible cooling effect to the rotor hub as described by Horwood et al. [19]. Understanding the radial migration of the egressed air is important for efficient engine design of downstream hardware. Circumferential traverses downstream of the turbine blades were performed to quantify how far away from the inner turbine wall there is a presence of egressed flow from the wheelspace cavity.

Two flow configurations were used to trace how the cooling flow exiting the upstream wheelspace migrates into the main gas path, configuration (6) and (7) in Table 3. The first configuration was set up to vary the VTE flow while holding purge flow constant, referred to as *VTEMigration*. The purge flow chosen for this first configuration was that corresponding to a fully sealed wheelspace, i.e. $\varepsilon_{cc} = 1.0$ at $\Phi_P/\Phi_{ref} = 1.2$ as was shown in Figure 9. The vane trailing edge flow rate was varied from $\Phi_{VTE}/\Phi_{ref} = 0$ to 0.7. The second configuration holds the VTE flow rate constant at $\Phi_{VTE}/\Phi_{ref} = 0.4$ while varying the purge flow rate from $\Phi_P/\Phi_{ref} = 0.3$ to 1.2. The second configuration was referred to as *PurgeMigration*. Both flow configurations were seeded using the *Purge+VTE* elevated 1.0% CO_2 seeding configuration to study the combined migration of purge and VTE flow into the main gas path.

A full vane pitch of equally spaced circumferential increments was traversed downstream of the turbine and the collected data was arithmetically averaged in the circumferential direction. A common cooling flow condition was chosen for comparison across the two flow configurations. This common radial profile was chosen to be at $\Phi_P/\Phi_{ref} = 1.2$ purge flow rate and $\Phi_{VTE}/\Phi_{ref} = 0.4$ VTE flow rate, which corresponds to the blue curve with filled triangles in both Figure 14 and Figure 15. One full vane pitch of data was collected at 0.1 vane pitch increments, as well as a total of 22 points in the radial direction were collected. A higher number of points were collected near the inner diameter wall to better resolve the gradient of CO_2 egressed from the wheelspace cavity that migrates along the inner turbine wall as described by Scobie et al. [18]. Each radial location data point in the two figures is an average of the 10 pitch increment points that covered the full vane pitch in the circumferential direction.

To quantify the amount of CO_2 egressed from the wheelspace cavity, a local CO_2 concentration definition is required for the flow (as opposed to surface measurements, which were defined using ε). The CO_2 measured aft of the turbine disk in the main gas path is a direct measurement of the local flow field CO_2 concentration thus, a second non-dimensional parameter, θ, is used as shown in Equation (3). The non-dimensional parameter, θ, is analogous to a non-dimensional temperature of cooling in the main gas path. A value of $\theta = 100\%$ corresponds to a full presence of purge and VTE flow in the main gas path, whereas, a value of $\theta = 0\%$ means no purge and VTE flow in the main gas path.

$$\theta = \frac{c - c_{\infty,in}}{c_s - c_{\infty,in}} \approx \varepsilon_{cc} \tag{3}$$

Figure 14 and Figure 15 show circumferentially averaged radial traverses of CO_2 concentration in the main gas path. Both figures are plotted so that the vertical axis in Figure 14 shows the pitch-

averaged traverse results for the *VTEMigration* configuration. The three circumferentially averaged profiles in Figure 14 exhibit similar radial shape, in which high CO_2 concentration was measured near the inner diameter main gas path wall, and lower CO_2 values were measured with increasing radial location away from the inner wall. This corresponds to lower temperatures in the inner wall due to the high presence of CO_2 in the main gas path. Measurements in the outer wall show levels of CO_2 which correspond to decreased presence of purge flow since in both Figure 14 and Figure 15 VTE flow is used.

From Figure 14, it can be observed that as the VTE flow is increased the local CO_2 concentration in the main gas path increases. This trend was expected since the wheelspace is fully purged for this configuration, and the VTE flow is minimally ingested. As stated previously in Figure 10, as purge flow increases the amount of VTE flow ingested into the wheelspace cavity decreases. The linear shift of each curve presented in Figure 14 is a direct consequence of increasing the VTE flow rate which raises the contribution of CO_2 in the main gas path.

Figure 15 shows the circumferentially averaged results for the *PurgeMigration* configuration. By holding the VTE flow rate constant, a decrease in purge flow rate causes all three curves in Figure 15 to collapse to approximately $\theta = 8\%$ as radial span increases. This $\theta = 8\%$ is due to the constant VTE contribution to CO_2 levels in the main gas path. The outer radial region CO_2 concentrations for all three cases are within the uncertainty levels of the gas analyzers. Results in Figure 15 show that θ levels was not found to linearly shift with increasing purge flow as shown in Figure 14. As purge flow is increased, the range of θ increases in the inner wall region which contributes to a cooled inner wall as purge flow increases. When the purge flow is lowered, the VTE flow and main gas path ingestion becomes dominant in the wheelspace cavity, as was shown

in Figure 10. Decreasing the purge flow rate, produces less egress from the wheelspace cavity which decreases the presence of CO_2 which contributes to a hotter inner wall.

To compare the effects of the variation of the purge and VTE flows, area averaged CO_2 concentration levels were plotted versus the total cooling mass flow, Φ_{TCF}. The total cooling flow is defined as the total combined amount of purge and VTE flow as given by Equation (4).

$$\Phi_{\mathrm{TCF}} = \Phi_{\mathrm{P}} + \Phi_{\mathrm{VTE}} \tag{4}$$

Figure 16 shows the area-averaged CO_2 concentrations ($\bar{\bar{\theta}}$) with respect to the total cooling flow into the turbine vane. It can be observed that for the flow configuration where the VTE flow rate is held constant at $\Phi_{\mathrm{VTE}}/\Phi_{\mathrm{ref}} = 0.4$ and purge flow varies (*PurgeMigration*) the area averaged θ values do not significantly change as the total cooling flow increases, for the range of total cooling flow shown in Figure 16. However, it can be observed in Figure 15 that the θ value near the inner wall decreases as purge flow decreases. For the case where VTE flow varies while purge flow is held constant at the fully purged condition, *VTEMigration*, the $\bar{\bar{\theta}}$ increases in an approximately linear trend. This is due to increased VTE flow rate which increases the presence of CO_2 throughout the main gas path which causes a linear shift as shown in Figure 14 as well as Figure 16.

From the flow migration study presented above, it can be observed that flow egressed from the wheelspace has a tangible presence in the main gas path which can extend to up to 50% of the main gas path radial span. Flow egressed from the wheelspace cavity is entrained into the passage vortex with positive cooling effect to the rotor hub as shown by Horwood et al. [19]. The addition of VTE flow further improves this cooling potential in the main gas path.

CONCLUSIONS

While rim seal flows have been extensively studied, the effect of engine-realistic vane trailing edge flows on ingestion have not been studied. This more realistic boundary condition is important to understanding the relevant physics that lead to efficient cooling and optimal use of existing cooling flows. To determine the effects of how vane trailing edge flow influences the rim cavity cooling effectiveness, seven different CO_2 seeding cases were defined that allowed the main gas path flow, the vane trailing edge flow, and purge flow to each be distinguished from one another.

The experimental results presented in this paper definitively show that the vane trailing edge flows have a significant influence in the rim seal performance. In fact, the results indicated that the vane trailing edge flow can be ingested into the wheelspace region resulting in additional cool air being entrained under the platform. High fidelity CFD URANS simulations confirms that VTE flow can be found as deep as the front wheelspace cavity region. Simulations also show the mixing, recirculation zones and flow streamlines in the hub, and rim seal cavity. The results also showed that as the purge flow decreased, the vane trailing edge flow became a dominant influence on the cooling effectiveness levels. A simple linear superposition of the individual cooling flow contributions to the rim cavity cooling effectiveness measurements was found to exist.

Circumferentially averaged radial traverses of the main gas path CO_2 concentration levels were performed downstream of the turbine to track the radial flow migration. A constant purge flow with varying vane trailing edge flow and a constant vane trailing edge flow with a varying purge flow were investigated. Both cases indicated a high concentration of CO_2 near the inner diameter turbine wall.

For the fully sealed condition, no vane trailing edge flow entered the wheelspace, which was verified both through the circumferential traverse averages of the main gas path flow field

concentration as well as the local measured concentration levels in the wheelspace. Alternatively, as the purge flow is decreased below the fully sealed condition, the vane trailing edge flow influence increased resulting in vane trailing edge flow being ingested into the wheelspace cavity.

The results from this study point to the importance of considering how all of the various flows bled from the compressor are used in the turbine thereby warranting a more systems-based approach as compared to individual components. This investigation also points to the importance of using engine-realistic hardware operated at relevant conditions.

ACKNOWLEDGMENTS

The authors would like to thank Pratt & Whitney and the U.S. Department of Energy National Energy Technology Laboratory for sponsoring research presented in this paper. This paper is based upon work supported by the Department of Energy under Award Number DE-FE0025011.

Disclaimer: "This report was prepared as an account of work sponsored by an agency of the United States Government. Neither the United States Government nor any agency thereof, nor any of their employees, makes any warranty, express or implied, or assumes any legal liability or responsibility for the accuracy, completeness, or usefulness of any information, apparatus, product, or process disclosed, or represents that its use would not infringe privately owned rights. Reference herein to any specific commercial product, process, or service by trade name, trademark, manufacturer, or otherwise does not necessarily constitute or imply its endorsement, recommendation, or favoring by the United States Government or any agency thereof. The views and opinions of authors expressed herein do not necessarily state or reflect those of the United States Government or any agency thereof."

NOMENCLATURE

b	Hub radius
C	Chord length
c	Gas concentration
$\dot{m}$	Mass flow rate
PR	Stage pressure ratio
s_C	Seal clearance
Re_x	Axial Reynolds number, VC_x/ν
Re_ϕ	Rotational Reynolds number, $\Omega b^2/\nu$
T	Temperature
V	Main gas path velocity
ε_c	Sealing effectiveness, $(c - c_\infty)/(c_s - c_\infty)$
ε_{cc}	Cooling effectiveness, $(c - c_{\infty,in})/(c_s - c_{\infty,in})$
υ	Kinematic viscosity
Ω	Angular velocity
Φ	Cooling flow rate, $\dot{m}/(2\pi s_c \rho \Omega b^2)$
Φ_0	Largest flow parameter with zero effectiveness
Φ_{min}	Minimum flow parameter to seal a given location
Φ_{ref}	Reference flow rate, Φ_{min} for Location B at Baseline
ρ	Density
θ	Local CO_2 concentration in MGP

Subscripts, Accents, and Abbreviations

in	Inlet conditions
MGP	Main gas path
P	Purge
ref	Generic reference condition
s	Supply level
TCF	Total cooling flow
t	Total condition
VTE	Vane trailing edge
x	Axial direction
∞	Background level
¯	Area averaged value

REFERENCES

[1] Scobie, J. A., Sangan, C. M., Owen J. M., and Lock G. D., 2016, "Review of Ingress in Gas Turbines", *ASME J. Eng. Gas Turb. Power*, **138**(12), p. 120801.

[2] Johnson, B. V., Mack, G. J., Paolillo, R. E., and Daniels, W. A., 1994, "Turbine Rim Seal Gas Path Flow Ingestion," AIAA Paper No. 94-2703

[3] Bayley, F., J. and Owen, J. M., 1970, "The Fluid Dynamics of a Shrouded Disk System with a Radial Outflow of Coolant", *J. Eng. Power*, **92**(3), pp. 335–341.

[4] Phadke, U. P. and Owen J. M., 1988, "Aerodynamic Aspects of the Sealing of Gas Turbine Rotor-Stator Systems – Part 1: The Behavior of a Simple Shrouded Rotating-Disk Systems in a Quiescent Environment", *Int. J. Heat Fluid Flow*, **9**(2), pp. 98 – 105.

[5] Phadke, U. P. and Owen J. M., 1988, "Aerodynamic Aspects of the Sealing of Gas Turbine Rotor-Stator Systems – Part 2: The Performance of Simple Seals in a Quasi-Axisymmetric External Flow", *Int. J. Heat Fluid Flow*, **9**(2), pp. 106 – 112.

[6] Phadke, U. P. and Owen J. M., 1988, "Aerodynamic Aspects of the Sealing of Gas Turbine Rotor-Stator Systems – Part 3: The Effect of Nonaxisymmetric External Flow on Seal Performance", *Int. J. Heat Fluid Flow*, **9**(2), pp. 113 – 117.

[7] Owen J. M., 2011, "Prediction of Ingestion through Turbine Rim Seals: Part II, Externally-Induced and Combined Ingress", *ASME J. Turbomach.*, **133**(3), p. 031006.

[8] Owen, J. M., Zhou, K., Pountney, O. J., Wilson, M., and Lock, G., 2012, "Prediction of Ingress through Turbine Rim Seals - Part I: Externally Induced Ingress," *ASME J. Turbomach.*, **134**(3), p. 031012.

[9] Sangan C. M., Pountney, O. J., Zhou, K., Wilson, M., Owen, J. M. and Lock, G. D., 2013, "Experimental Measurements of Ingestion through Turbine Rim Seals – Part I: Externally-Induced Ingress", *ASME J. Turbomach.*, **135**(2), p. 021012.

[10] Barringer, M., Coward, A., Clark, K., Thole, K., Schmitz, J., Wagner, J., Alvin, M. A., Burke P., and Dennis, R., 2014, "Development of a Steady Thermal Aero Research Turbine (START) for Studying Secondary Flow Leakages and Airfoil Heat Transfer", ASME Turbo Expo 2014, Paper No. GT2014-25570, Dusseldorf, Germany.

[11] Clark, K., Barringer, M., Thole, K., Clum, C., Hiester, P., Memory, C., and Robak, C., 2017, "Effects of Purge Jet Momentum on Sealing Effectiveness," *ASME J. Eng. Gas Turb. Power*, **139**(3), p. 031904.

[12] Clark, K., Barringer, M., Johnson, D., Thole, K., Grover, E., and Robak, C., 2018, "Effects of Purge Flow Configuration on Sealing Effectiveness in a Rotor-Stator Cavity," *ASME J. Eng. Gas Turb. Power,* **140**(11), p. 112502.

[13] Berdanier, R. A., Monge-Concepción, I., Knisely, B. F., Barringer, M. D., Thole, K. A., and Grover, E. A., 2019, "Scaling Sealing Effectiveness in a Stator–Rotor Cavity for Differing Blade Spans," *ASME. J. Turbomach.*, **141**(5), p. 051007.

[14] Gentilhomme, O., Hills, N. J., Turner, A. B., and Chew, J. W., 2003, "Measurement and Analysis of Ingestion Through a Turbine Rim Seal," *ASME. J. Turbomach.*, **125**(3), p. 505–512.

[15] Scobie, J. A., Sangan, C. M., Owen, J. M., Wilson, M., Lock, G. D., 2014, "Experimental Measurements of Hot Gas Ingestion through Turbine Rim Seals at Of-Design Conditions,", *Proc. Inst. Mech. Eng. Part A J. Power Energy*, **228**(5), p. 491 – 507.

[16] Patinios, M., Scobie, J. A., Sangan, C. M., and Lock, G. D., 2017, "Performance of Rim-Seals in Upstream and Downstream Cavities over a Range of Flow Coefficients," *Int. J. Turbomach. Propuls. Power*, **2**(4), p. 21.

[17] Patinios, M., Ong, I. L., Scobie, J. A., Lock, G. D., and Sangan, C. M., 2018, "Influence of Leakage Flows on Hot Gas Ingress," *ASME. J. Eng. Gas Turbines Power*; **141**(2), p. 021010.

[18] Scobie, J. A., Hualca, F. P., Patinios, M., Sangan, C. M., Owen, J. M., and Lock, G. D., 2018, "Re-Ingestion of Upstream Egress in a 1.5-Stage Gas Turbine Rig," *ASME J. Eng. Gas Turb. Power*, **140**(7), p. 072507.

[19] Horwood, J. T. M., Hualca, F. P., Wilson, M., Scobie, J. A., Sangan, C. M., and Lock, G. D., 2018, "Unsteady Computation of Ingress Through Turbine Rim Seals," *ASME Turbo Expo 2018*, Paper No. GT2018-75321

[20] Mee, D. J., Baines, N. C., Oldfield, M. L. G., and Dickens, T. E., 1992, "An Examination of the Contributions to Loss on a Transonic Turbine Blade in Cascade." *ASME. J. Turbomach.*, **114**(1), p. 155–162.

[21] Aminossadati, S. M., and Mee, D. J., 2013, "An Experimental Study on Aerodynamic Performance of Turbine Nozzle Guide Vanes with Trailing-Edge Span-Wise Ejection," *ASME. J. Turbomach.*, **135**(3), p. 031002.

[22] Clark, K., Barringer, M., Thole, K., Clum, C., Hiester, P., Memory, C., and Robak, C., 2016, "Using a Tracer Gas to Quantify Sealing Effectiveness for Engine Realistic Rim Seals," *ASME Turbo Expo 2016*, Paper No. GT2016-58095.

[23] Figliola, R. S., and Beasley, D. E., 2014, *Theory and Design for Mechanical Measurements*, John Wiley & Sons, Inc.

[24] Gao, F., Poujoul, N. P., Chew, J. W., and Beard, P. F., 2018, "Advanced Numerical Simulation of Turbine Rim Seal Flows and Consideration for RANS Turbulence Modelling," *ASME Turbo Expo 2018*, Paper No. GT2018-75116

[25] Siemens PLM Software, 2017, "STAR-CCM+ 11.06," Plano, TX, USA.

[26] ANSYS, 2017, "ANSYS Fluent 18.2," Canonsburg, PA, USA.

[27] Robak, C. W., Faghri, A., and Thole, K. A., 2019, "Analysis of Gas Turbine Rim Cavity Ingestion with Axial Purge Flow Injection," *ASME Turbo Expo 2019*, Paper No. GT2019-91807

List of Tables

Table 1. Turbine Operating Conditions

Parameters	Value
Vane Inlet Mach Number	0.1
Vane Inlet Axial Reynolds Number, Re_x	1.1×10^5
Blade Inlet Axial Reynolds Number, Re_x	1.1×10^5
Rotational Reynolds Number, Re_ϕ	$4.0 - 9.6 \times 10^6$
Density Ratio, ρ_P/ρ_{MGP}	1.0 – 2.0
Relative Purge Flow Rate, Φ_P/Φ_{ref}	0.1 – 1.3
Relative Purge Flow Rate, Φ_{VTE}/Φ_{ref}	0.1 – 0.7

Table 2. Measurement Uncertainties

Parameter	Value
Main gas path flow rate, $\dot{m}/\dot{m}_{ref}$	±0.004
Shaft rotational speed, Ω/Ω_{ref}	±0.001
Pressures, P/P_{ref}	±0.001
Temperatures, T	±0.04 K
1.0 stage pressure ratio, PR/PR_{ref}	±0.005
Purge flow rate, $\dot{m}_P/\dot{m}_{ref}$	±0.018
Cooling effectiveness, ε_{cc}	±0.015 to ±0.025

Table 3. CO_2 Seeding Configurations and Cooling Flow Setpoints

CO_2 Seed Configuration	MGP Background CO_2 Level	Purge Flow CO_2 Level	VTE CO_2 Level	Φ_P/Φ_{ref}	Φ_{VTE}/Φ_{ref}
(1) Baseline	0.2%	1.0%	No Flow	0.1 – 1.3	No Flow
(2) Purge	0.2%	1.0%	0.2%	0.1 – 1.3	0.4
(3) Purge+VTE	0.2%	1.0%	1.0%	0.1 – 1.3	0.4
(4) VTE1	0.2%	0.2%	1.0%	0.1 – 1.3	0.4
(5) VTE2	0.2%	0.2%	1.0%	0.4	0.1 – 0.7
(6) VTEMigration	0.2%	1.0%	1.0%	1.2	0.0 – 0.7
(7) PurgeMigration	0.2%	1.0%	1.0%	0.3 – 1.2	0.4

List of Figure Captions

Figure 13. Superposition relationship between seeding configurations.

Figure 14. Circumferentially averaged radial traverses for *VTEMigration* study.

Figure 15. Circumferentially averaged radial traverses for *PurgeMigration* study.

Figure 16. Constant VTE flow with varying purge flow (1) and constant purge with varying VTE flow (2) local CO_2 growth trends.

FIGURES

Fig. 1 START facility and measurement equipment.

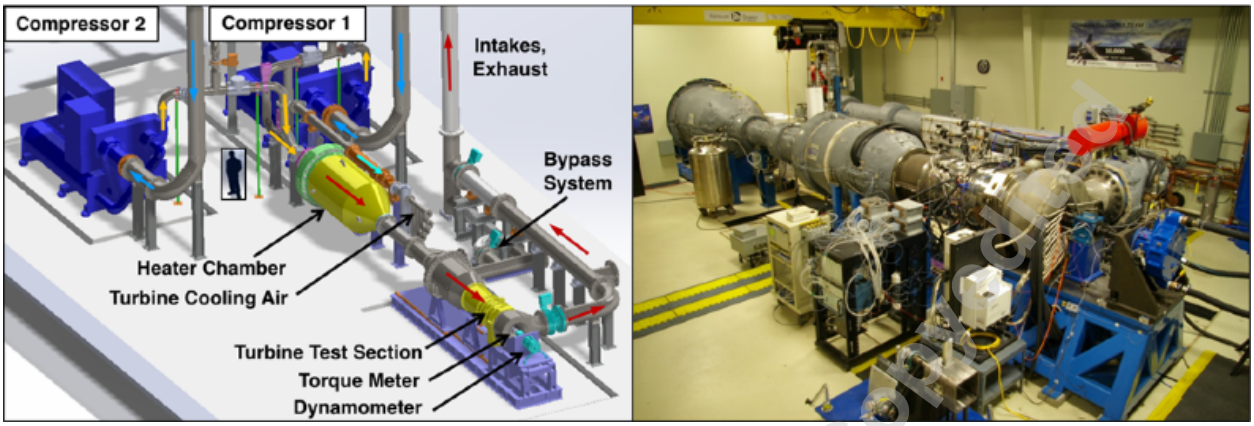

Fig. 2 Cross-section diagram showing the turbine main gas flow path and secondary flows

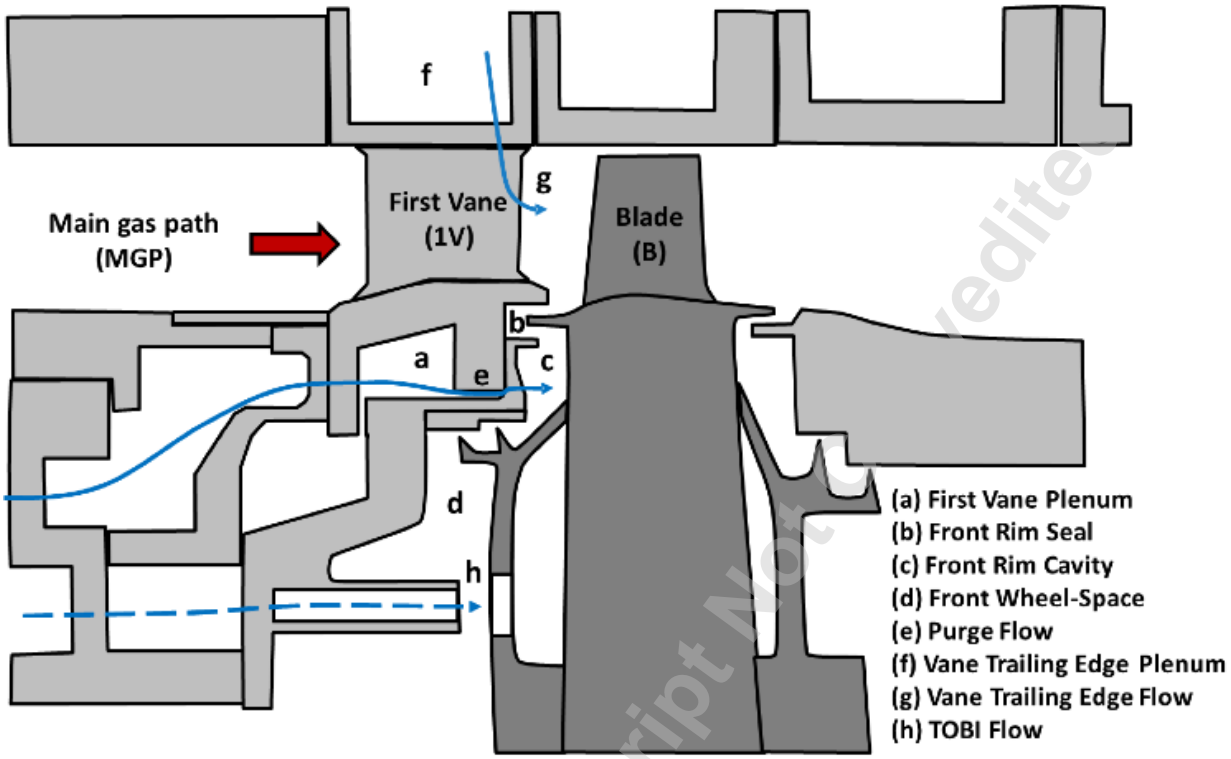

Fig. 3 Test section instrumentation

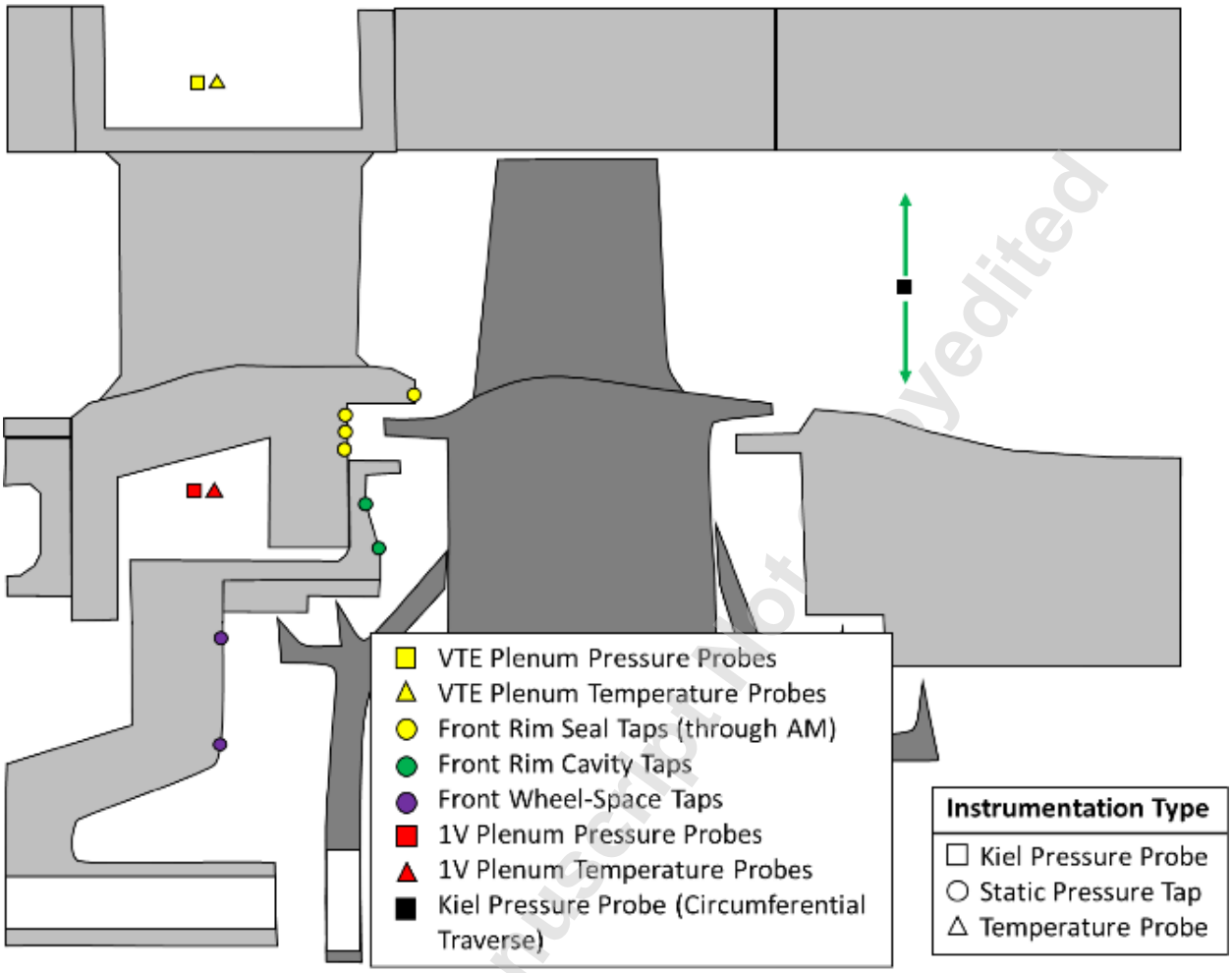

Fig. 4 CO_2 injection and sampling system

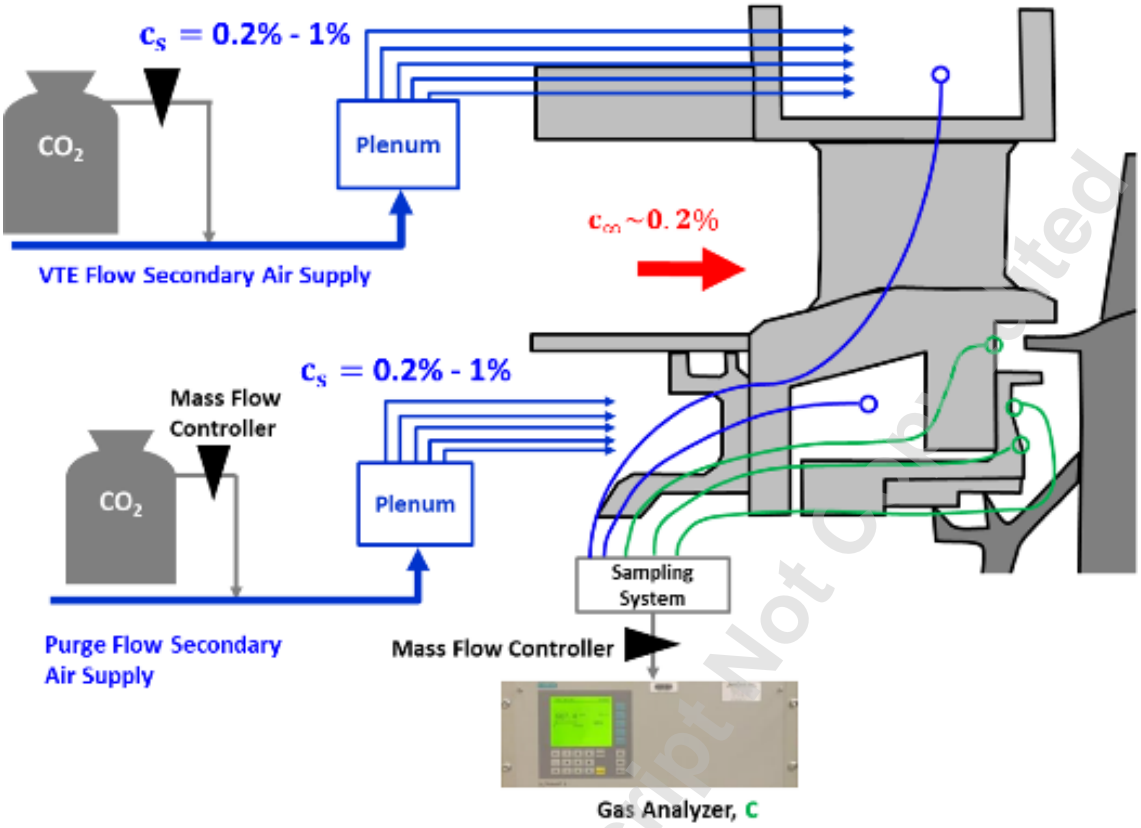

Fig. 5 Rim seal test locations and cooling flows

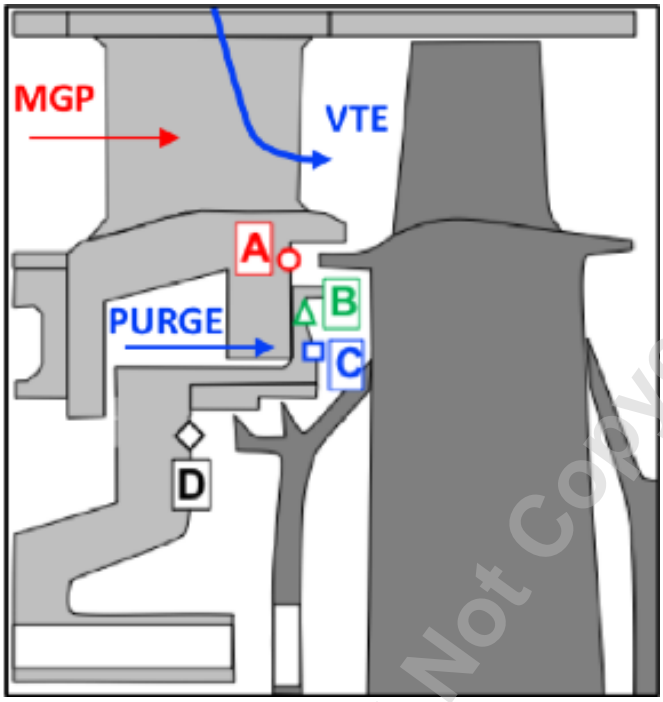

Fig. 6 CO_2 Seeding Configurations: (1) *Baseline* Configuration, (2) *Purge* Configuration, (3, 6, 7) *Purge+VTE, VTEMigration,* and *PurgeMigration* Configurations, (4, 5) *VTE1* & *VTE2* Configurations.

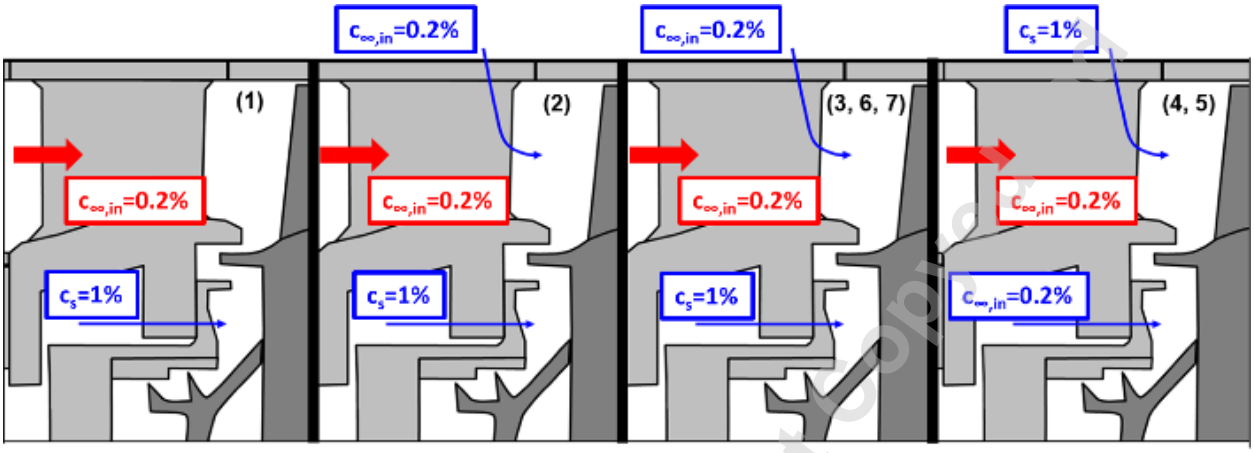

Fig. 7 Comparison of rim sealing effectiveness for the *Baseline* and previous results from Berdanier et al. [13]. Open symbols are for the *Baseline* while solid symbols are for previous results.

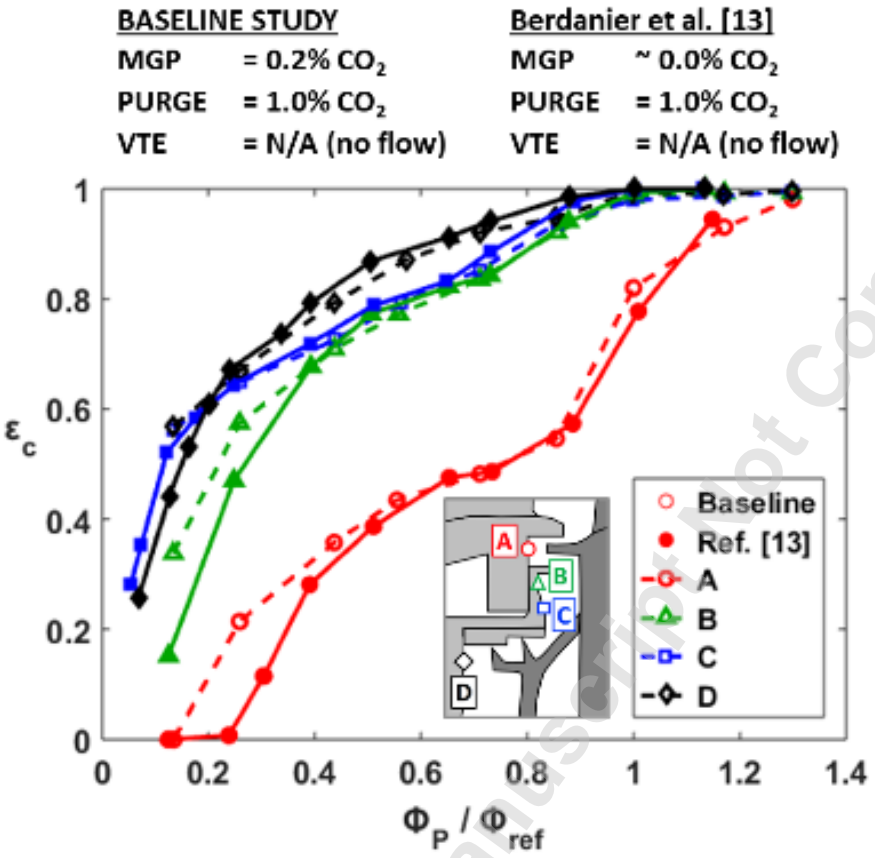

Fig. 8 Comparison of rim cavity cooling effectiveness for the *Baseline* and *Purge* cases. Open symbols are for the *Baseline* while the solid symbols are for the *Purge* case.

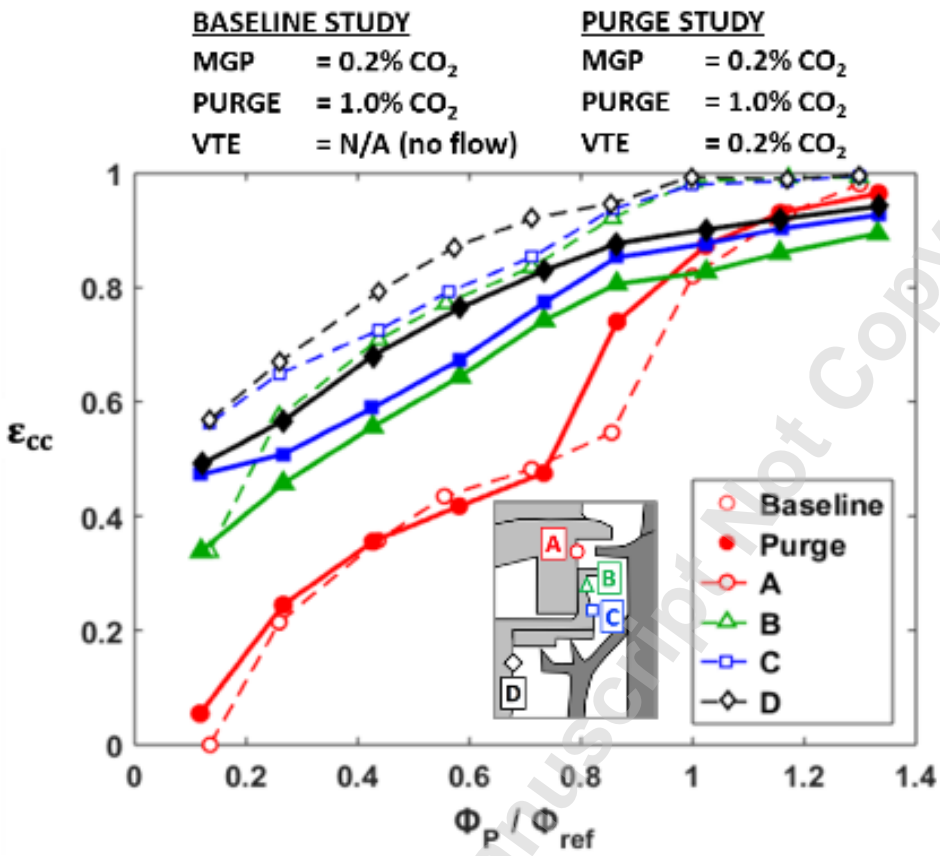

Fig. 9 Rim cavity cooling effectiveness results for the *Purge+VTE* CO_2 seeding configuration compared with the *Baseline* results.

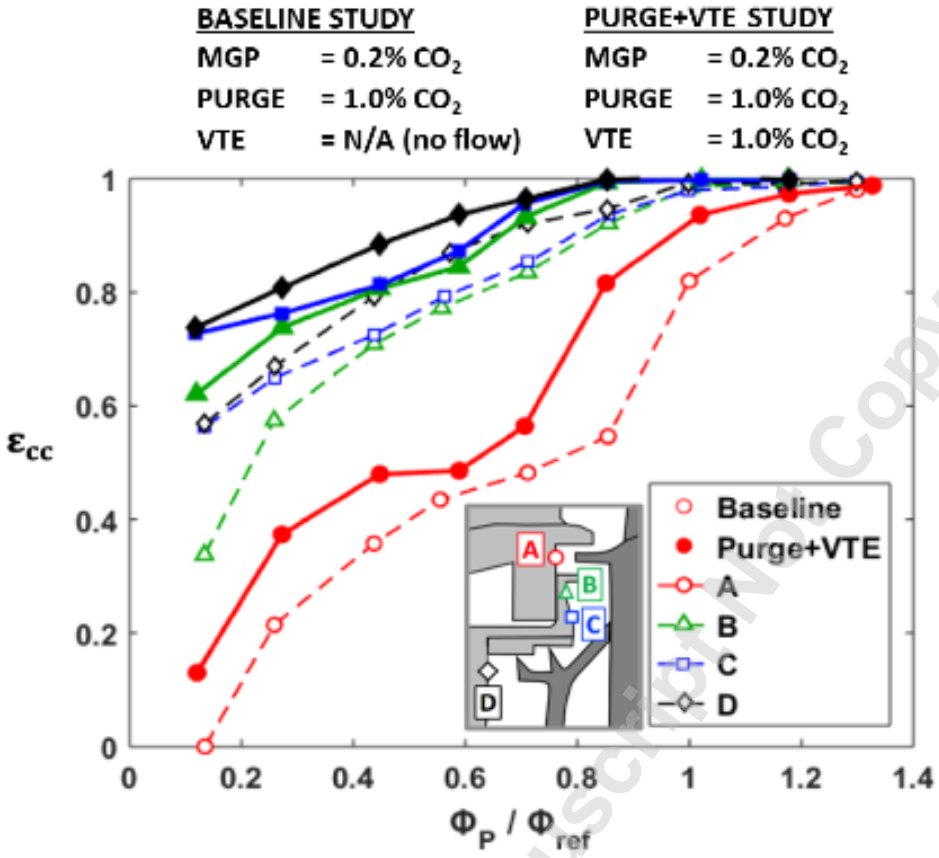

Fig. 10 Rim cavity cooling effectiveness results for the *VTE1* CO_2 seeding configuration.

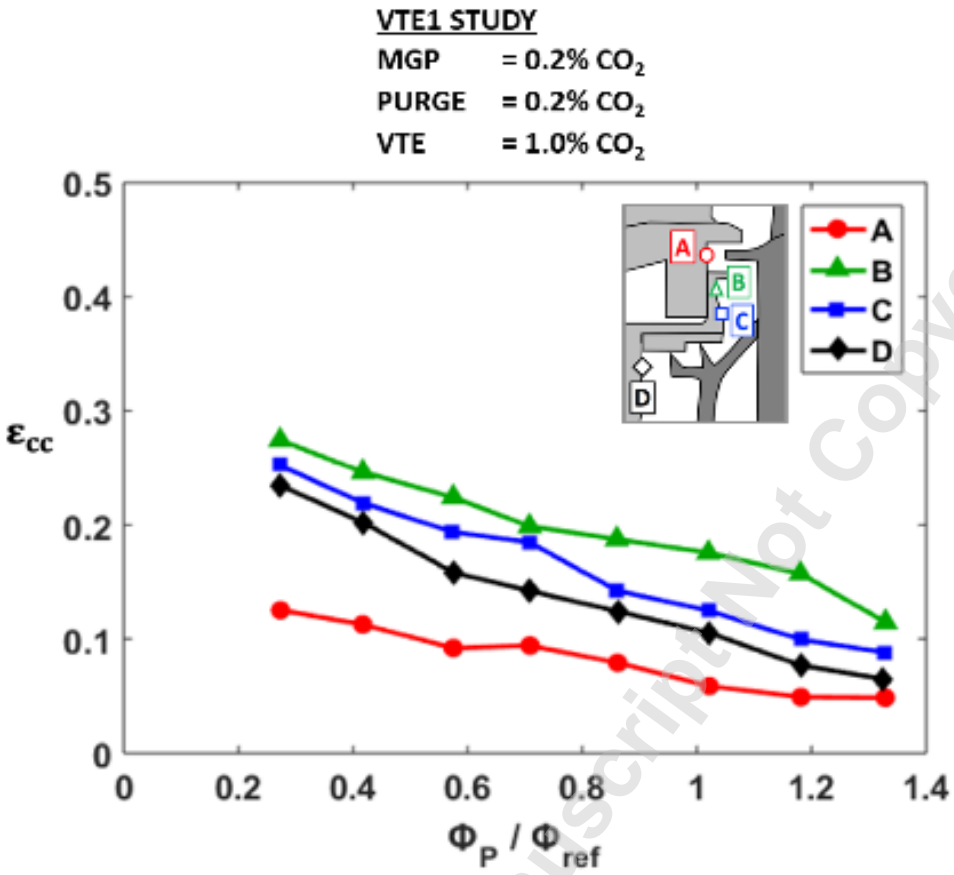

Fig. 11 Rim cavity cooling effectiveness results for *VTE2* CO_2 seeding configuration.

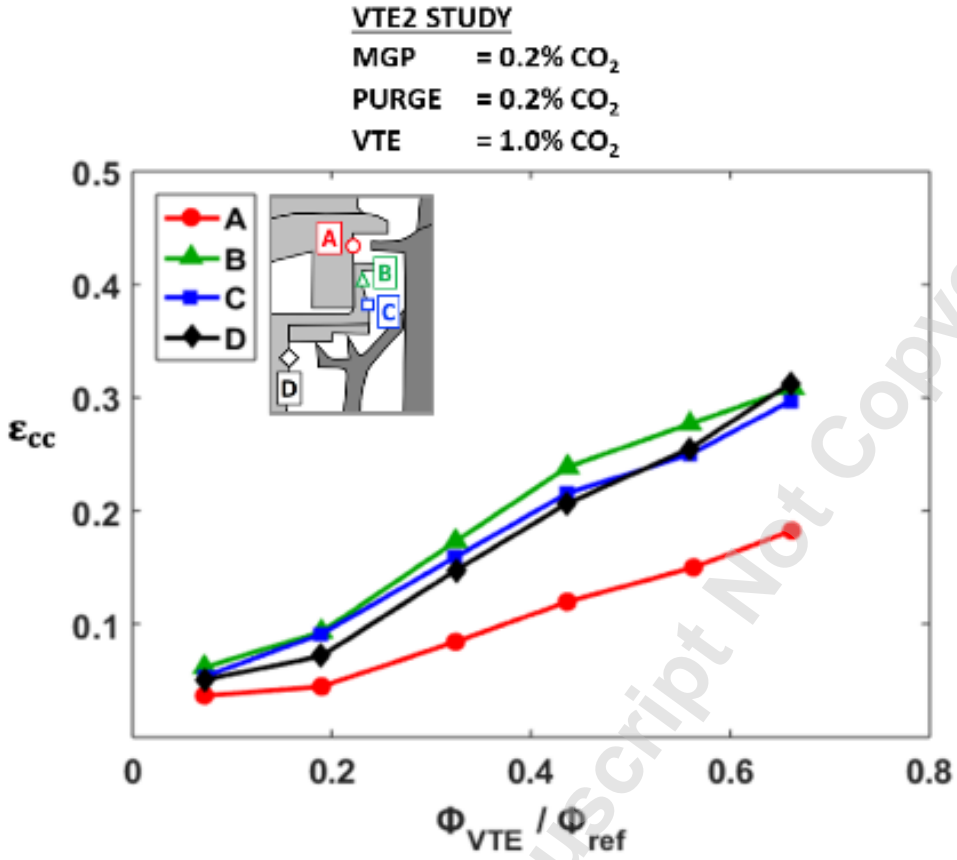

Fig. 12 CFD simulation results illustrating the ingestion of vane trailing edge flow in the rim seal and cavity regions ranging from highest concentration (high) to lowest concentration (blue). (a) Isometric view and (b) cross-section view of main gas path and rim cavity regions.

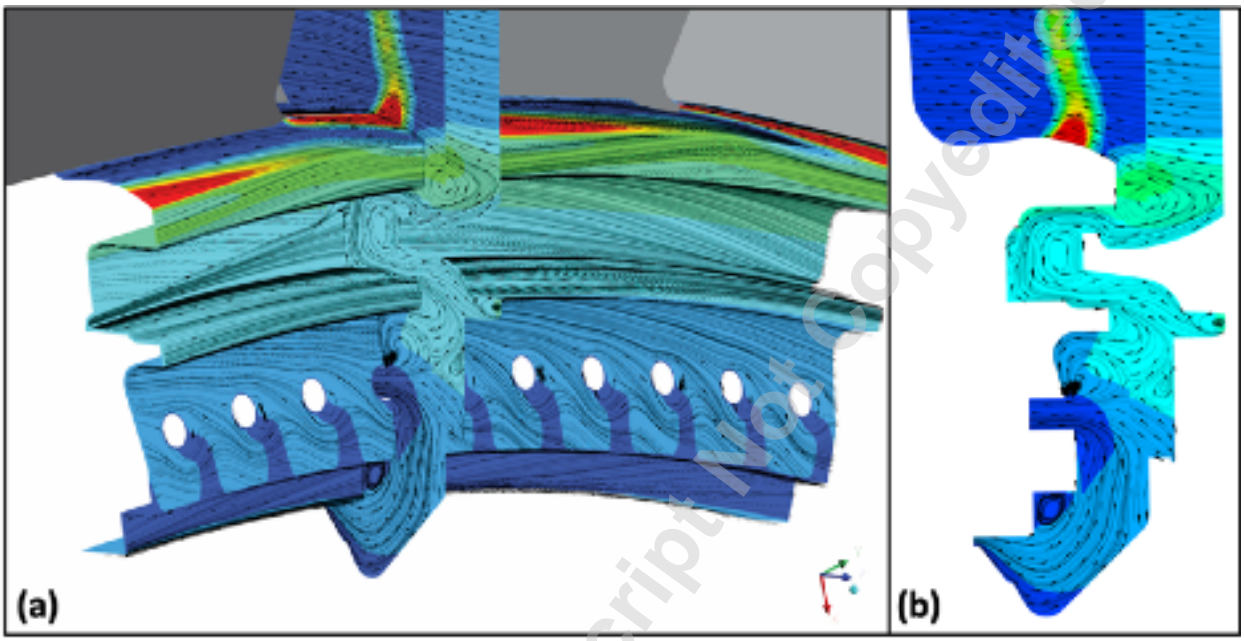

Fig. 13 Superposition relationship between seeding configurations.

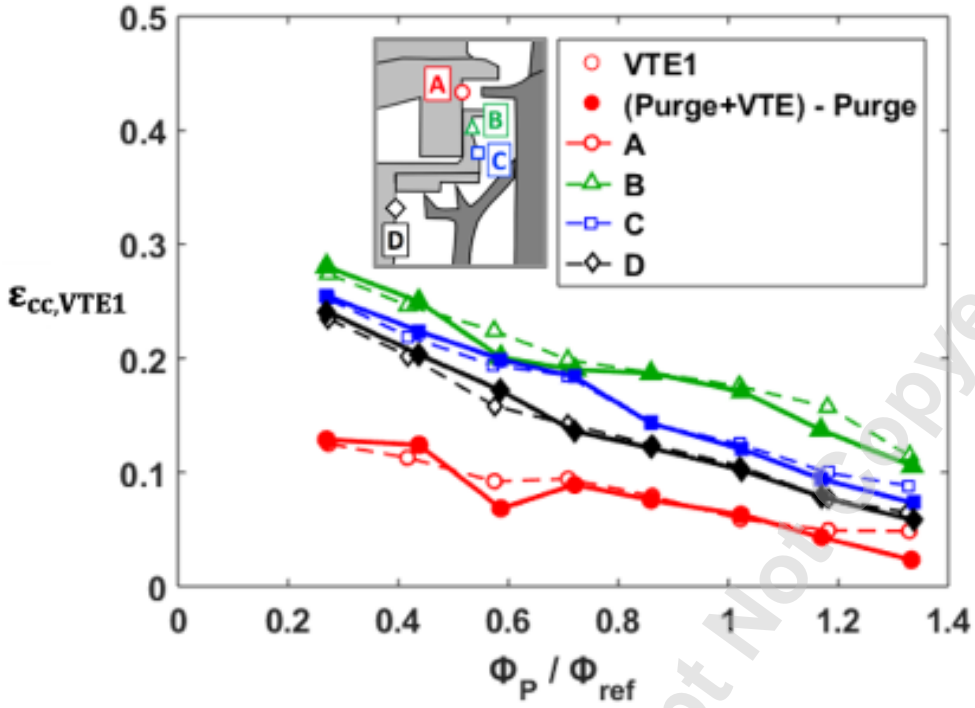

Fig. 14 Circumferentially averaged radial traverses for *VTEMigration* study.

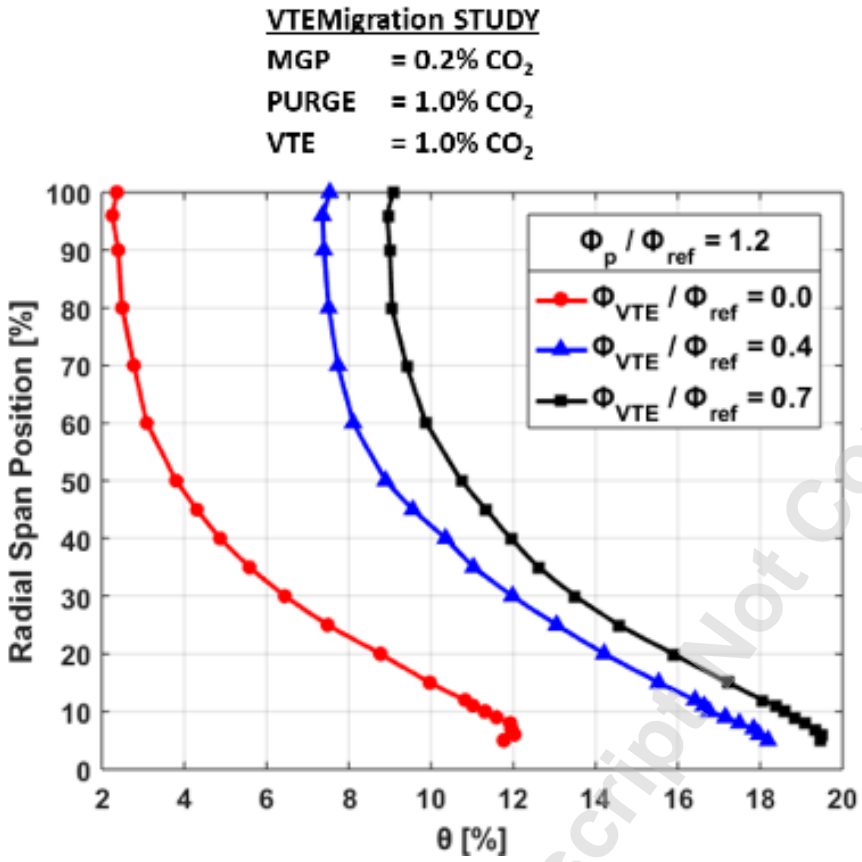

Fig. 15 Circumferentially averaged radial traverses for *PurgeMigration* study.

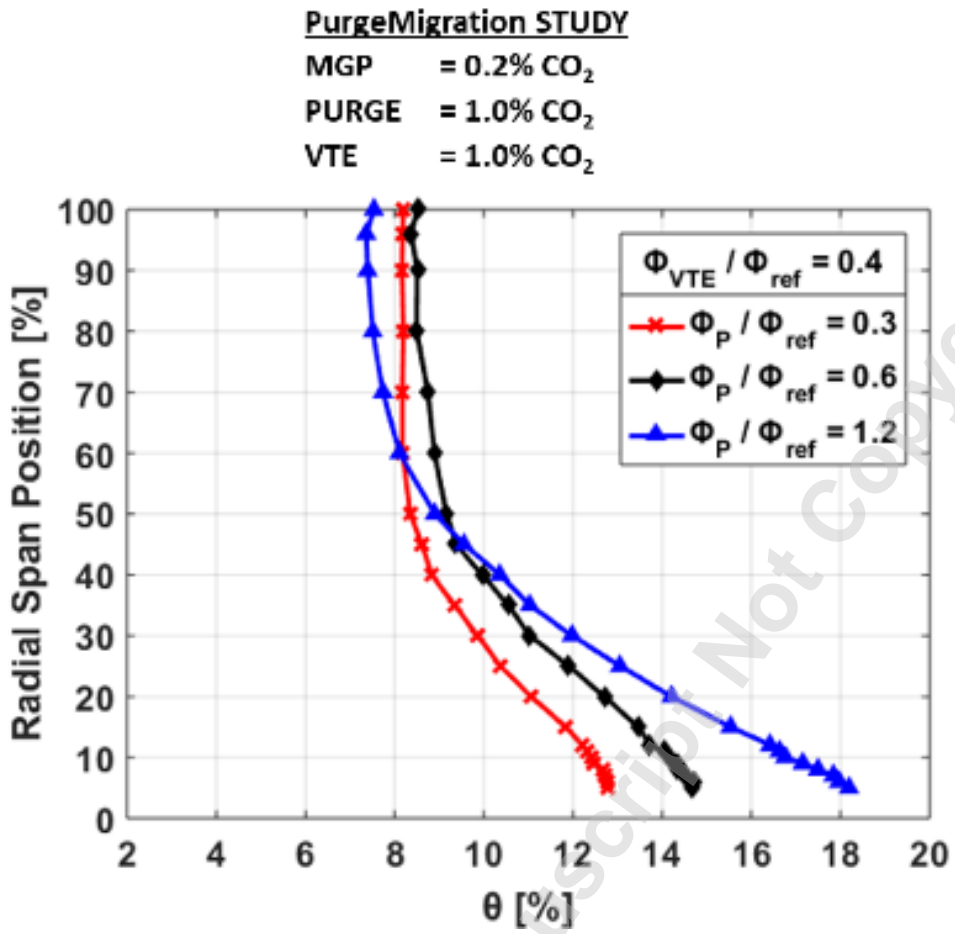

Fig. 16 Constant VTE flow with varying purge flow (1) and constant purge with varying VTE flow (2) local CO_2 growth trends.